

See discussions, stats, and author profiles for this publication at: <https://www.researchgate.net/publication/221805332>

Hyperbranched Polyglycerols as Trimodal Imaging Agents: Design, Biocompatibility, and Tumor Uptake

ARTICLE in BIOCONJUGATE CHEMISTRY · FEBRUARY 2012

Impact Factor: 4.51 · DOI: 10.1021/bc200280g · Source: PubMed

CITATIONS

21

READS

67

9 AUTHORS, INCLUDING:



[Kelly C McPhee](#)

University of Alberta

14 PUBLICATIONS 29 CITATIONS

[SEE PROFILE](#)



[Jennifer H E Baker](#)

University of British Columbia / BC Cancer Res...

29 PUBLICATIONS 409 CITATIONS

[SEE PROFILE](#)



[Stefan A Reinsberg](#)

University of British Columbia - Vancouver

51 PUBLICATIONS 950 CITATIONS

[SEE PROFILE](#)



[Urs O Häfeli](#)

University of British Columbia - Vancouver

94 PUBLICATIONS 2,448 CITATIONS

[SEE PROFILE](#)

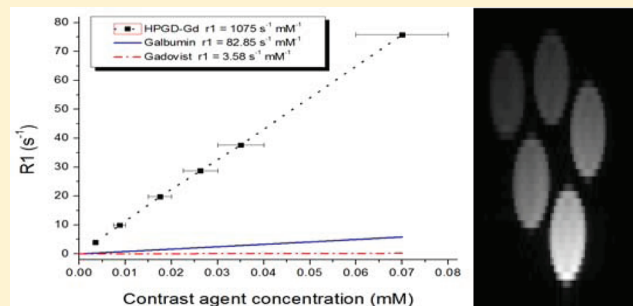
Hyperbranched Polyglycerols as Trimodal Imaging Agents: Design, Biocompatibility, and Tumor Uptake

Katayoun Saatchi,[†] Peter Soema,[†] Nikolaus Gelder,[†] Ripen Misri,[†] Kelly McPhee,[‡] Jennifer H.E. Baker,[‡] Stefan A. Reinsberg,[‡] Donald E. Brooks,[§] and Urs O. Häfeli*,[†]

[†]Faculty of Pharmaceutical Sciences, [‡]Department of Physics, and [§]Centre for Blood Research, University of British Columbia, Vancouver, British Columbia, Canada

Supporting Information

ABSTRACT: Combining various imaging modalities often leads to complementary information and synergistic advantages. A trimodal long-circulating imaging agent tagged with radioactive, magnetic resonance, and fluorescence markers is able to combine the high sensitivity of SPECT with the high resolution of MRI over hours and days. The fluorescence marker helps to confirm the *in vivo* imaging information at the microscopic level, in the context of the tumor microenvironment. To make a trimodal long-circulating probe, high-molecular-weight hyperbranched polyglycerols (HPG) were modified with a suitable ligand for ¹¹¹In radiolabeling and Gd coordination, and additionally tagged with a fluorescent dye. The resulting radiopharmaceutical and contrast agent was nontoxic and hemocompatible. Measured radioactively, its total tumor uptake increased from 2.6% at 24 h to 7.3% at 72 h, which is twice the increase expected due to tumor growth in this time period. Both *in vivo* MRI and subsequent histological analyses of the same tumors confirmed maximum HPG accumulation at 3 days post injection. Furthermore, Gd-derivatized HPG has an excellent contrast enhancement on T1-weighted MRI at 10× lower molar concentrations than commercially available Galbumin. HPG derivatized with gadolinium, radioactivity, and fluorescence are thus long-circulating macromolecules with great potential for imaging of healthy and leaky blood vessels using overlapping multimodal approaches and for the passive targeting of tumors.



INTRODUCTION

Over the past few decades, imaging has become a vital tool for cancer research, clinical diagnosis, and treatment. Various imaging techniques such as MRI (magnetic resonance imaging), SPECT (single photon emission computed tomography), PET (positron emission tomography), and others have grown tremendously and are widely applied in medicine.¹ These techniques are useful for locating tumors and investigating various biological processes. They each possess different characteristics regarding spatial resolution, depth penetration, tissue contrast, time needed for imaging, and cost. To overcome specific limitations, it is becoming increasingly common to combine several imaging modalities. Multimodality imaging allows for the visualization of pharmacokinetics, and helps to elucidate complicated mechanisms of drug uptake and/or action, and processes that influence tumor behavior. As a result of multimodal imaging, there is an increasing need for multimodal contrast agents.

This report summarizes our findings on the use of a macromolecule as a suitable platform for multimodal imaging. Our focus on a macromolecular agent is partly motivated by a long-standing problem in the MR imaging of tumor vasculature: uptake of low-molecular-weight agents currently used in dynamic contrast-enhanced imaging always yields data

that can be interpreted as a combination of both tumor perfusion and extravasation. This is the result of the typically leaky vasculature located in tumors, such that low molecular weight agents expected to remain intravascular in other tissues actually leak out of the tumor vasculature and can accumulate in the extravascular space.^{2,3} A higher molecular weight contrast agent that could be expected to remain intravascular even within leaky tumor vasculature would yield data that could be interpreted more specifically to represent the physiological parameters of permeability and perfusion.

Hyperbranched polyglycerols are recently described globular macromolecules with narrow size distribution.^{4,5} Kainthan et al. then developed in 2006 a one-pot synthesis method that extended the 30 kDa molecule narrow size distribution to larger than 100 kDa molecules.⁶ HPG have radii of 5–10 nm, are highly water-soluble, are easily made by a one-step synthesis, unlike the otherwise similar dendrimers,⁷ are somewhat asymmetrical, and are highly biocompatible.^{8–11} Their biocompatibility is similar to that of poly(ethylene glycol) (PEG)¹² or polysaccharides. HPG, however, is thermally and

Received: June 1, 2011

Revised: January 30, 2012

Published: February 6, 2012

oxidatively more stable than the linear PEG, and produces less viscous solutions at analogous molecular weights due to its globular structure. HPGs are thus useful over larger concentration ranges and behave more like proteins than PEG.⁹ Already tested applications of HPGs are as human serum substitute,¹³ as drug delivery vehicles for the treatment of bladder cancer,^{14,15} and as a protectant of cell surfaces.^{16,17}

Many macromolecules have been modified for use in imaging and tumor targeting. We were interested in investigating HPG as a potential new tracer and smart nanoprobe for the characterization of vessel leakiness and perfusion with multimodal imaging techniques. For this purpose, HPG was modified with radioactive, MRI contrast enhancing, and fluorescent tags, and thus became a bioprobe for detection with SPECT, MRI, and fluorescent imaging. Having multiple probes on the same carrier molecule is preferred and obviates the need to administer two or more compounds with somewhat different pharmacokinetics. *In vivo* MR imaging of the Gd-labeled HPG can yield physiologically relevant data regarding vascular function, while SPECT allows to quantitatively assess the agent's biodistribution over time. The microregional location of the agent within the tumor microenvironment, including for how long the agent remains intravascular, can be determined at the microscopic level using the fluorescent tags imaged using fluorescence microscopy. Together, these data can provide specific insight regarding the physiological function of tumor blood vessels.

To prepare the radioactive and magnetic compound, the chelator 1,4,7,10-tetraazacyclododecane-1,4,7,10-tetraacetic acid (DOTA) was used to prepare the radioactive and paramagnetic probes as it coordinates both In³⁺ and Gd³⁺ metal ions with good stability. HPG was also modified with a fluorescent dye which made it possible to observe the distribution of HPG at the end of the experiment *ex vivo* using fluorescence microscopy. The gamma emitting isotope ¹¹¹In ($t_{1/2} = 67$ h; $\gamma = 172$, and 245 keV) has ideal characteristics for extended investigation of slowly clearing compounds and is commonly used for SPECT imaging. For MR imaging, however, Gd complexes are commonly used as contrast agents. The R1 relaxation rate of water in tissue is increased with Gd, and the presence of Gd can thus be qualitatively and quantitatively assessed *in vivo*.

The trimodal HPG described here was used for biodistribution analyses by radiation and MR imaging, as well as for more exact fluorescent tumor tissue distribution studies with histological methods. The multifunctional nature of the HPG nanoprobe allows for more complete investigation of observed effects at different time points and resolutions. Syntheses and characterization of the trimodal HPG, as well as metal coordination/radiolabeling, biodistribution, and MR and fluorescent tumor imaging studies are reported herein.

MATERIALS AND METHODS

All chemicals were purchased from Sigma/Aldrich. ¹¹¹InCl₃ was purchased from MDS Nordion (Ottawa, ON, Canada). Alexa Fluor 647 and fluorescamine were purchased from Invitrogen (Carlsbad, CA, USA), while *p*-NH₂-Bn-DOTA came from Macrocylics (Houston, TX, USA). ¹H NMR spectra were recorded on a Bruker AV-300 or AV-400 at 300.13 or 400.13 MHz. Inductive coupled plasma (ICP) analyses were obtained from Exova (Surrey, BC, Canada). Molecular weights and polydispersities of polyglycerol samples were determined by gel permeation chromatography (GPC) on a Waters 2690

separation module fitted with a DAWN EOS multiangle laser light scattering (MALLS) detector from Wyatt Technology Corp.⁶ Sephadex G-25 M columns (i.e., PD10; contains 0.15% Kathon CG as preservative) were from GE Healthcare (Piscataway, NJ, USA). Instant thin layer chromatography (ITLC) was performed on green TEC-Control strips (Cat# 150–771; Bidex, Shirley, NY, USA) using a 33.3% mixture of saline, HCl (0.1 M), and Na₂EDTA (0.1 M) as the mobile phase. Dialysis tubing was from SPECTRUM laboratories (Rancho Dominguez, CA, USA) with MWCO of 1000. The radioactive TLCs were made visible using a phosphor imager (Cyclone with 12.5 × 25 cm² phosphor screen, Perkin-Elmer, Waltham, MA, USA) and analyzed using OptiQuant software. Ultracel-YM100 microconcentrators with a 100 kDa MWCO were from Millipore Corporation (Billerica, MA, USA). Fresh blood was obtained from healthy volunteers immediately before the hemocompatibility studies. Results are the average of at least triplicate repetitions.

HPG. The high-molecular-weight polyglycerol (HPG) was synthesized in Brook's laboratories with a narrow polydispersity of PDI = 1.01 by ring-opening multibranching polymerization of glycidol using dioxane as the reaction medium, according to a published procedure.⁶ ¹H NMR (D₂O): δ 3.3–3.9 (br, m, [−CH₂−CHCH₂−OH−O]_n), GPC: M_n 509 kDa. For spectra, see Supporting Information (SI).

Ligand Modified HPG (HPGD). HPG was dissolved (353 mg, 0.76 μ mol) in 5 mL of water. A solution of H₅IO₆ (24.4 mg, 107 μ mol) in 1 mL water was added dropwise with stirring. After 1 h the solution was dialyzed against 2.5 L water overnight, and water was changed once. *p*-NH₂-Bn-DOTA (46 mg, 63 μ mol) was dissolved in 5 mL water, added to the reaction mixture in a round-bottom flask, and stirred for 1 h. Ethanolamine (90 μ L, 10% solution, 1.5 mmol) was added and stirred for another 1 h. NaBH₃CN (excess, 18 mg, 286 μ mol) was dissolved in 100 μ L water and added (pH ~ 5), followed by acetic acid to decrease the pH to 3. The solution was stirred overnight, dialyzed for 3 days against water with daily water changes, and then lyophilized. ¹H NMR (D₂O): δ 2.2–3.8 (b, overlapping multiplets, HPG [−CH₂−CHCH₂−OH−O]_n, DOTA N-CH₂CH₂-N and N-CH₂-COOH), 7.0 (d, DOTA CH₂-C₆H₅). GPC: M_n 583 kDa, PDI = 1.07. For spectra, see SI.

HPGD-NH₂. In a 50 mL round-bottom flask, HPG (247 mg, 0.5 μ mol) was dissolved in 10 mL of water and 5 mL H₅IO₆ solution (101 mg, 442 μ mol) added dropwise with stirring. After 1 h, the solution was dialyzed against water for 2 days and water was changed 3 times. *p*-NH₂-Bn-DOTA (112.5 mg, 155 μ mol) was dissolved in 5 mL water and added to the reaction mixture after transferring back to the flask and stirred for 1 h. N-Boc-ethylenediamine (24 mg, 150 μ mol) was dissolved in 500 μ L of ethanol and added. After 1 h, ethanolamine (400 μ L, 10% (V/V) solution, 660 μ mol) was added and stirred for another 1 h. NaBH₃CN (50 mg, 794 μ mol) was dissolved in 1 mL of water, added to the reaction mixture (pH ~ 6), and pH adjusted to 5 with acetic acid and then stirred overnight. The reaction mixture was dialyzed for 4 days against water with daily fresh water and finally lyophilized to collect 207 mg of HPGD-NHBoc. For deprotection, 86 mg of HPGD-NHBoc was dissolved in HCl (1.25 M in MeOH) and stirred at 1000 rpm for 5 days. The solution was diluted with water (50%) and dialyzed for 3 days against 2.5 L of water (water changed twice daily). A fluffy white solid (HPGD-NH₂) was collected after lyophilization (81 mg). Quantification of NH₂ was by using a ninhydrin assay according to published literature using

ethanolamine as standard; each sample was measured in triplicate.^{18,19} The standard plot of absorbance versus concentration of different dilutions for ethanolamine was then used to calculate the concentration of amine functionality on the HPGD-NH₂ to be 2680 nmol NH₂ per mg HPGD.

Fluorescent HPGD (HPGDF). For quick examination of the free amine groups, 30 μL of HPGD-NH₂ solution (1.7 mg/100 μL 0.2% NaCl solution) was added to 50 μL of fluorescamine (3 mg/mL in dry acetone) in triplicate.²⁰ The fluorescence of each sample was read in a plate reader upon excitation at 390 nm and emission at 470 nm (57803 ± 382 RFU vs 812 ± 14 RFU for the background). The background was corrected against a mixture of fluorescamine solution and 0.2% NaCl. For *in vivo* experiments, a more stable fluorescent HPG was prepared. HPGD-NH₂ (75 mg) was dissolved in 2 mL borate buffer 0.1 M and 400 μL of the succinimidyl ester of Alexa647 in DMSO (1 mg/mL) was added and shaken overnight in the dark at 500 rpm on an Eppendorf thermomixer at 22 °C. The blue solution was purified and washed three times in a microconcentrator, and collected in 200 μL of saline. The fluorescence emission of HPGDF was checked at 668 nm. The fluorescence was 500 times relative to background.

Gd Coordination. To a solution of HPGD (or HPGDF) was added GdCl₃·6H₂O (1.14 mg per 5 mg of HPGD), and it was heated at 70 °C for 30 min in a thermomixer at 1000 rpm. After cooling to room temperature, the excess Gd was removed either by dialysis or by using a microconcentrator. ICP: [Gd]/mg HPG found 20.2 μg (calculated 21.72 μg). The fluorescence of HPGDF-Gd after metal coordination (5400 RFU vs 7 for background) was very similar to the starting HPGDF.

¹¹¹In-HPGD. To a solution of HPGD (0.5 mg/5 μL water) was added ¹¹¹InCl₃ (5 μL, 8.40 MBq) and the volume made up to 500 μL with NH₄OAc (0.15 M). After 30 min shaking at 70 °C, the solution was cooled to room temperature. A 250 μL aliquot was placed on a PD10 column and eluted with 30 × 500 μL aliquots of saline. The activity of each fraction was measured in a gamma-counter. Fractions from 2 to 5 mL were combined and contained the ¹¹¹In-HPG, while the fraction between 6 and 8 mL contained the so-called “free” activity. The peak between instant thin layer chromatography was also used on the original mixture, the images developed using a phosphor imager first, and then the ITLCs were cut and the two parts were counted in the gamma-counter. Labeling efficiency was >95%.

¹¹¹In-HPGDF. To prepare a fluorescent radiolabeled product, the above procedure was performed with HPGDF instead of HPGD with similar labeling results (>95%).

EDTA Challenge. To determine the binding stability of the metals to the HPG derivative, Na₂EDTA (750 μL, 0.1 M) was added to the remaining solution of ¹¹¹InHPGD (250 μL, 4.07 MBq) and the solution heated at 37 °C while shaking. At 1 and 24 h post mixing, 250 μL samples of this solution were eluted on a PD 10 column.

Transferrin Challenge. A HPGD solution (1 mg/10 μL H₂O) in 490 μL of NH₄OAc (0.15 M) with ¹¹¹InCl₃ (5 μL, 9.88 MBq) was shaken at 1000 rpm on a thermomixer for 30 min at 99 °C. Apotransferrin solution in PBS (2.5 mg/mL; 500 μL) was added to 250 μL of this solution. The solution was shaken on a mixer at 1000 rpm at 37 °C. At 1 and 24 h, 370 μL of the solution was separated in a microconcentrator and the activity measured for both the supernatant and the ¹¹¹In-HPGD.

Cell Viability Assay (MTT Assay). A quantitative analysis of cell viability was performed with HPG and HPGD in human

vascular endothelial cells (HUVECs) using 3-(4,5-dimethylthiazol-2-yl)-2,5-diphenyltetrazolium bromide assay (MTT assay).²¹ The cells (100 μL, 5000 cells/mL) were plated into 96-well plates and incubated at 37 °C and 5% CO₂ for 2 days. HPGD and HPG at concentrations 10, 2, 1, 0.5, and 0.1 mg/mL were added in 100 μL of medium (EBM-2 Basal Medium, Lonza) to the wells and incubated for 24 h. MTT stock solution (5 mg/mL; 20 μL) was added to each well, incubated for 3 h, the supernatant gently removed, and 150 μL DMSO added to every well. The plate was shaken at 1000 rpm and at 37 °C for 1 h and the optical density measured at 540 nm on a Multiscan Ascent plate reader.

RBC Aggregation Test. Red blood cell (RBC) aggregation was tested by incubating whole blood with HPGD, Gd-HPGD, and HPG. HPGs (10 μL, 10 mg/mL) were added to 40 μL citrate anticoagulated whole blood and incubated at 37 °C for 30 min. The RBC were then isolated by spinning down the blood for 30 s. Plasma (4 μL) was resuspended and diluted such that single RBC or aggregations were visible under the bright field light microscope (Zeiss Axioskop 2plus). A drop was placed on a wet-mounted slide and images were taken with a mounted black and white CCD camera (Qimaging Retiga 1300).

Clinical Coagulation Assays. Prothrombin time (PT) and activated partial thromboplastin time (APTT) were measured to evaluate the influence of the HPG solutions on extrinsic and common coagulation pathway of blood (ST4 Diagnostica Stago device). A polymer solution (1 mg/mL) was prepared in platelet poor plasma (PPP) and 3× 100 μL of it heated to 37 °C; Innovin (200 μL, for the PT assay) or actin and calcium chloride (100 μL each, for the APTT assay) were incubated with PPP and the time to fibrin clot formation recorded. The PPP was produced by spinning down whole blood at 1500 g for the maximum time of 15 min and the plasma was separated from the RBC. Each measurements contained 3 samples of polymer/PPP and one plasma control. The experiment was repeated 3 times.

Thrombelastograph (TEG). The platelet function and mechanical clot stability was analyzed in a thrombelastograph (TEG) hemostasis system 5000 (Hemoscope Corp, Niles, IL, USA). The TEG measures the physical properties of the clot in an oscillating cylindrical cup holding the blood sample, at an angle of 4°45'. Each of the rotational cycles lasted 10 s and the properties were measured by a stationary pin. Fresh citrated blood (360 μL) was mixed with 40 μL of the polymer test solutions (1 mg/mL) and CaCl₂ (20 μL, 0.2 M) added in the thrombelastograph and the resulting curves analyzed by TEG's proprietary software.

Complement Activation. The complement activation pathway of the body upon exposure to the polymers was investigated using the Quidel C3a enzyme immunoassay kit.²² For this purpose, samples (1 mg/mL) and controls were diluted 1:100 with sample buffer and added to a 96 microassay plate coated with C3a antibody coated strips. After 60 min of incubation at room temperature, 100 μL of C3a conjugate was added into each well. After 60 min the substrate was added and incubated for another 15 min. The reaction was then stopped and read at 450 and 650 nm on a plate reader.

Platelet Activation. Platelet activation, which is the tethering of platelets occurring on sites of vascular injuries, was investigated by measuring the CD62 expression level in the blood by marking it with CD62 mouse human antibodies.²³ Fresh donated citrate anticoagulated blood was centrifuged at

800 g (900 rpm) for 30 s to separate the RBCs from the plasma without spinning down the platelets to get Platelet Rich Plasma (PRP). PRP (150 μ L) was then incubated at 37 °C with 15 μ L of the polymer solutions to obtain a final concentration of 1 mg/mL. Aliquots were withdrawn after 10, 30, and 60 min; 5 μ L was added to 45 μ L of PBS and 5 μ L of CD62 mouse human antibodies and analyzed in the flow cytometer. As a positive control, 45 μ L of PBS was mixed with 5 μ L of PRP, 5 μ L of CD62 mouse human antibodies (Immunotech, Marseille France), and 5 μ L of Gly-Pro-Arg-Pro (GPRP). To prove that platelets were present in the PRP, CD42 antibodies were added instead of CD62.

Radioactive Biodistribution Studies. To assess the organ uptake of HPG radiolabeled with a gamma emitter, a biodistribution study was performed at the animal resource center of the BC Cancer Research Centre (BCCRC) in accordance with an approved animal protocol. The female C57BL/6 mice aged 6–8 weeks (Jackson Laboratory, Bar Harbor, ME, USA) were injected subcutaneously with 3×10^5 LL/2 (Lewis Lung) tumor cells (CRL-1642, American Type Culture Collection (ATCC), Manassas, VA, USA) in 50 μ L of media (DMEM supplemented with 4 mM L-glutamine, 4.5 g/L glucose, and 10% fetal bovine serum) into the flanks of the animals. Once the tumors reached a size of about 6 mm in diameter, 0.5 mg of ^{111}In -HPG (74 kBq) in 200 μ L of sterile phosphate buffered saline pH 7.4 was injected intravenously into the tail vein of 2 groups of 5 animals each. Groups were sacrificed at 24 and 72 h and organs were removed, weighed, and their activity determined using a Packard Cobra II auto gamma counter with settings for ^{111}In (energy window 140–280 keV). Results were corrected for blood content according to the method by Bally et al. and then expressed as the percentage of the injected dose per gram of tissue (%ID/g).²⁴

In Vivo Imaging and Histological Tumor Micro-distribution Studies. To assess the feasibility of HPGDF as an MR contrast agent, the R1 relaxation rate of HPGDF was measured in a buffer solution at concentrations between 2 and 40 mg/mL at room temperature.

To assess tumor uptake and retention of HPGDF, an MRI study and subsequent histological analysis were performed. Experiments followed a protocol approved by the UBC Committee on animal care. Mice were anaesthetized with isoflurane throughout imaging and maintained at 37 °C body temperature. Six female NOD/SCID mice (bred and maintained in-house in accordance with the Canadian Council of Animal Care guidelines) with HT29 human colorectal carcinoma (ATCC) xenografts were randomly assigned to three groups. All mice were injected with a dose of 300 or 600 mg/kg of HPGDF via the tail vein. Groups 1 and 2 received intravenous HPGDF injections while MR imaging was performed on a 7 T Bruker Biospec 70/30 using a combination of volume (T_x)/surface (R_x) coils. T_1 measurement and T_1 -weighted images were obtained. The first group was euthanized at 60 min post injection without waking from anesthesia. The second group was reimaged 3, 6, and up to 14 days post injection, and euthanized following the final imaging. Animals in the third group received HPGDF via intravenous injection and were euthanized 2 min following injection, without obtaining MR images. All tumors were excised immediately following euthanasia, and were frozen for subsequent cryosectioning.

For histological analysis, 10 μ m cryosections from the same central region of each tumor as imaged with MRI were

obtained and imaged for native fluorescence (625 nm) using a robotic microscope and camera to obtain tiled images of whole tumor sections. Images for individual tumors were cropped to tumor tissue boundaries, with artifacts and nonviable tissue removed using *ImageJ* software.²⁵ Whole tumor section fluorescence was measured as a reflection of contrast agent accumulation in tumor tissue, and was normalized by subtracting native tissue fluorescence background levels of tumors without HPGDF. Differences in fluorescence due to different doses were corrected for by assuming a linear relationship between dose and fluorescence.

MR Methods. The concentration-dependent ability of HPGDF to increase the relaxation rates of the surrounding water protons can be described by

$$\Delta R_1 = r_1[\text{HPGDF}] \quad (1)$$

where r_1 is the relaxivity, ΔR_1 is the change in relaxation rate measured for the HPGDF solution compared to the solvent alone. Relaxation times were measured for each sample by a nonimaging inversion recovery experiment and converted to relaxation rates ($R_1 = 1/T_1$).²⁶

The MRI protocol consisted of axial RARE T_1 -weighted images for morphological reference and orientation, a variable flip angle experiment to obtain RF field maps (FLASH TR/TE = 400/2.75; FA = 125°, 180°, 215°; slice = 1 mm),²⁷ and a variable flip angle experiment to obtain T_1 (FLASH, TR/TE = 100/2.77; FA = 10°, 20°, 50°, 60°; slice = 1 mm), and a T_1 -weighted image (RARE TR/TE = 1300/7.5; FA = 180°; slice = 1 mm). Following these images, the contrast agent was injected, and approximately 40 min post-injection, the variable flip angle experiment and RARE T_1 -weighted imaging were repeated. Imaging on days following the agent injection consisted of the same imaging protocol, but without contrast injection, and the associated repeated T_1 and RARE images. There was no contrast injection or repeat imaging on those days.

MRI postprocessing was performed using NIH-*ImageJ*,²⁸ and *Matlab* v 7.8 (The MathWorks Inc., Natick, MA, U.S.A.). Regions of interest with axial morphological images depicting a central tumor area were drawn with *ImageJ* and transferred to variable-flip-angle FLASH images. T_1 maps were calculated from the variable flip angle experiment. Reported R_1 values are averages calculated from a slice selected in the central region of each tumor.

■ RESULTS AND DISCUSSION

Multimodality imaging can be highly valuable in elucidating complicated mechanisms of drug uptake and/or action. This report summarizes our findings on the use of our multimodal HPG as a suitable platform for combined imaging using SPECT, MRI, and fluorescence microscopy. These probes can be used individually or in combination with each other if/when required. Ultimately, the overlapping application of HPG using these modalities will provide physiologically specific information regarding biodistribution, tumor vascular function, and response to treatment in preclinical investigations. HPG was synthesized and modified with a ligand suitable to bind ^{111}In for SPECT and Gd for MR imaging. HPG was also simultaneously tagged with an Alexa dye as a fluorescent probe for fluorescence imaging, resulting in a multimodal probe.

The commercially available bifunctional chelator, DOTA, that was chosen for use here, has a high binding stability for trivalent metals,²⁹ reaching a pM of 23.9 for In^{3+} and a pM of 24 for Gd^{3+} .³⁰ Due to the rigid ring structure, its metal

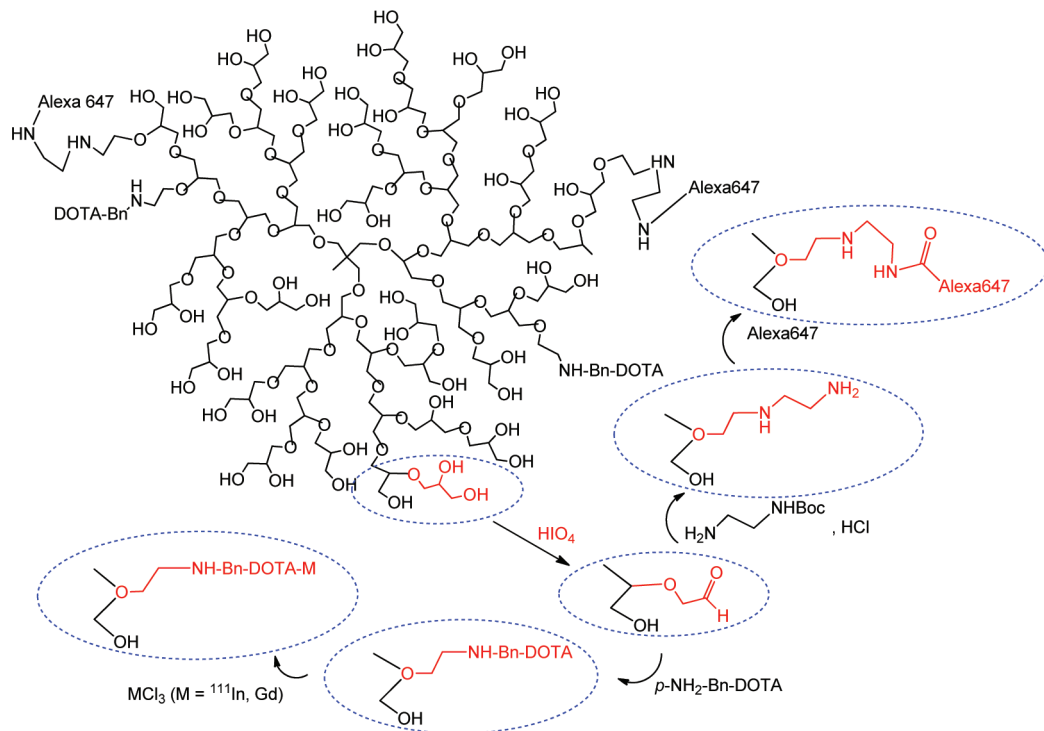


Figure 1. Synthetic scheme of HPG derivatization.

complexes tend to be kinetically inert to dissociation and are also highly thermodynamically stable.³¹ Since DOTA binds In³⁺ as well as Gd³⁺, and shows high reported *in vivo* stability for both metal complexes, we chose DOTA for HPG modification in our studies. The fact that the formation of DOTA metal complexes is kinetically slow³² was not a problem for our application, since heating does not degrade HPG.

The synthetic scheme for HPGD, HPGDF, and Gd/In-HPGDF is shown in Figure 1. Hydroxyl functionalities on HPG were oxidized to aldehyde and then coupled to *p*-NH₂-Bn-DOTA by reductive amination. To attach the fluorescent probe similar chemistry was carried to attach a linker arm (N-Boc-en) first. After Boc deprotection, the free amine was reacted with the activated fluorescent dye (succinimidyl ester of Alexa 647) to bind the fluorescent probe. The side product of the first reaction (i.e., formaldehyde) was removed by extensive dialysis. The product was then characterized by ¹H NMR and GPC indicative of a successful modification. Since there are no other aromatic protons in the structure but the ones of the benzyl backbone of DOTA, the appearance of the signal in the ¹H NMR spectrum of HPGD was a confirmation of ligand modification. Also, the ¹H NMR spectrum was used to calculate the number of DOTA groups attached (38 or 300 DOTAs per HPG) based on the integration ratio of the aromatic and aliphatic protons and the calculated total number of protons per HPGD molecule. Metal coordination was confirmed first using various concentrations of nonradioactive gadolinium. Measured by ICP, a [Gd³⁺] concentration of 20.2 µg per mg of HPG was found (calculated 21.72 µg) when excess Gd was added so that all DOTA groups were coordinated. Theoretically, both metal ions can be coordinated consecutively (partial coordination of DOTAs with Gd³⁺ first and then radiolabeling with ¹¹¹In³⁺ to coordinate the remaining DOTAs) if a SPECT/MR imaging is to be undertaken simultaneously. This was not attempted in this work.

Radiolabeling of HPGD with ¹¹¹In was performed with different concentrations as well (0.03 to 1 mCi/mg HPGD) at different temperatures (70–100 °C) for 30 min with excellent labeling efficiencies exceeding 95%. Figure 2 shows a typical

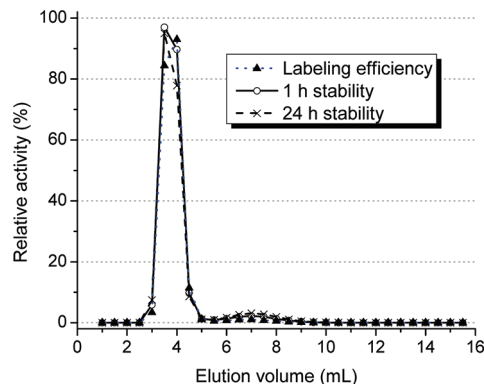


Figure 2. PD10 size exclusion trace of ¹¹¹In-HPGD directly after labeling (labeling efficiency) and after a stability challenge with EDTA 0.1 M at 1 and 24 h (stability), pointing to almost complete binding (peak at 4.0 mL) and very low instability (peak at 7.0 mL).

PD10 size exclusion profile of the radiolabeled HPGD. Almost all activity elutes in the first radioactive fraction around 4 mL, while only traces of activity are visible at 7.5 mL where In-EDTA would elute.

The stability of ¹¹¹In-HPGD for *in vivo* use was predicted by a challenge test with the competitive ligand ethylenediaminetetraacetic acid (EDTA). EDTA was chosen due to its log *K* of 25.3 for In, while In-DOTA has a log *K* of 23.9 and the physiologically present metal scavenger, transferrin, a log *K* of 18.30.³³ The EDTA challenge resulted in 94.9% and 92.7% of ¹¹¹In being HPGD bound after 1 and 24 h of incubation

(Figure 2), while the transferrin challenge resulted in 95.7% and 94.9% stability after 1 and 24 h.

To tag HPG with a fluorescent dye, a linker arm was attached with primary amine end groups (Figure 1). The use of a succinimidyl ester of Alexa dye was a simple way of coupling it to the amine groups on the HPG.

Toxicity of In-HPGD. Biocompatibility is extremely important for any pharmaceutical. To confirm the nontoxicity of our derivatives, we performed cell viability and hemocompatibility assays.

Cell Viability. After intravenous injection, the first cells that HPG come in contact with are the lining of the blood vessels and therefore the human vascular endothelial cells (HUVECs). To test for any potential cytotoxic effects of HPG and HPGD, we investigated HUVEC viability in an MTT assay (Figure 3).

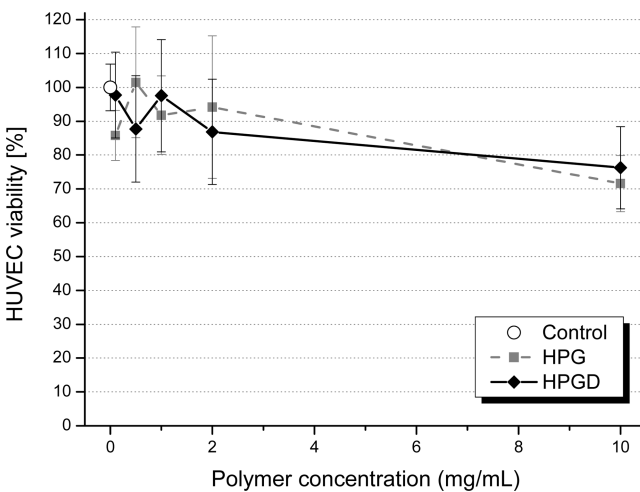


Figure 3. Cell viability of HUVECs after 24 h incubation with HPG and HPGD.

There was only a slight, nonstatistically significant cell viability loss at the highest polymer concentration of 10 mg/mL ($p = 0.485$ and $p = 0.138$, respectively). HPGD behaves thus almost identically to HPG, despite the additional free carboxyl and nitrogen groups on HPGD, and is considered to be biocompatible.

RBC Aggregation. Erythrocytes are a large group of cells in the human body which are in direct contact with any molecule injected into the bloodstream. They can aggregate naturally with molecules like fibrin as natural protection from injuries. Macromolecules such as antibodies and high-molecular-weight dextrans can also trigger this aggregation.^{9–22} The HPGD were tested by incubating the whole blood for 30 min with an added concentration of 10 mg/mL. No aggregation or cell shape change of RBC occurred as seen in Figure 4. Infrequent stacking, known as rouleaux, occurred because of the stop of motion, but could be disassembled easily by resuspension. The RBC shape thus was not changed indicating that the cells retain their functionality.³⁴

Clinical Coagulation Assays. The effect of the HPG derivatives at concentrations of 1 mg/mL on the common extrinsic (PT) and intrinsic (APTT) coagulation pathway was tested. All results were within normal ranges (30.4–31.1 s for APTT; 9.7–10.1 s for PT) and very close to the saline control (32.7 s for APTT (normal 30–45 s);³⁵ 10.1 s for PT (normal 10–13 s)³⁵). The derivatized HPG molecules thus do not

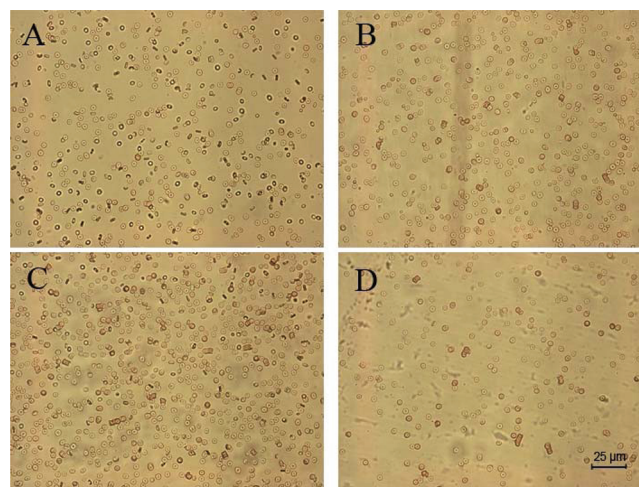


Figure 4. Microscopy pictures of red blood cells in the RBC aggregation assay. (A) HPG, (B) HPGD-Gd, (C) Control, (D) HPGD.

influence the fibrin clot formation and seem to be biocompatible.

Mechanical Blood Clot Properties. An additional blood biocompatibility test with a thrombolastograph (TEG) looked at other factors that influence the mechanical strength of the formed blood clot. The results in Figure 5 show a much broader variance than the other blood compatibility tests, but are certainly within normal values when compared to calibration data obtained from U.S. hospitals (thrombelastograph manual). The larger variances are due to the long duration of the test and the fact that fresh donor blood is required for each test, which made the use of different donors with individual clotting kinetics necessary.

Complement Activation. The nonspecific immune response expressed by complement activation was also investigated. This cascade of reactions involves C3 and a fragment C3a which act as diffusible signals for inflammatory response leading to cell lysis, clumping, phagocytosis, and chemotaxis.²² Measuring the concentration of C3a at two different time points and using inulin as a positive and EDTA as a negative control, both HPG and HPGD were shown to produce similar concentrations of C3a (Figure 6). No complement activation thus occurs with the chelating molecules present on the HPG surface.

Platelet Activation. The effect of HPG and derivatives on blood platelets was investigated by incubation with plasma followed by detection of the CD62 level, which is increased upon platelet activation.²³ Both derivatized and nonderivatized HPG slightly activated platelets to similar levels, as shown in Table 1. The values, however, showed fibrinogen binding levels below 10%, which is similar to that caused by saline⁹ and is still within the normal range, and could have been triggered by stress from shaking or pipetting.

Biodistribution. ¹¹¹In-HPGD is a long circulating blood pool agent with a biological half-life of 32.6 h. This result, however, is not very exact, as only two data points (59.6% of total injected activity in blood pool 24 h after injection, and 27.8% after 72 h) were available for the calculation. The rest of the activity was mainly found in organs of the reticuloendothelial system, the liver, and the spleen (Figure 7).

Tumor uptake was very similar to activity uptake in the reticulo-endothelial system, and the tumor to blood ratio increased in parallel from an earlier 0.295 to 0.891 at the later

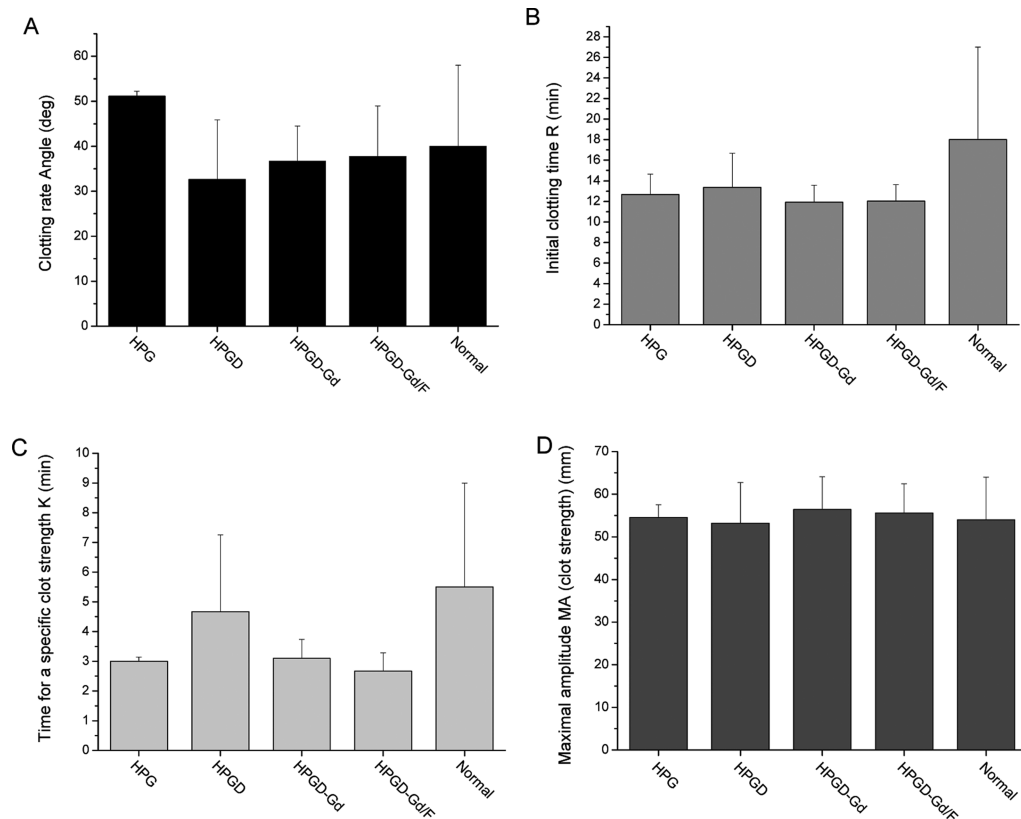


Figure 5. Diverse blood clotting parameters measured in whole blood with added HPG, HPGD, HPGD-Gd, and HPGD-Gd/F (1 mg/mL) using a Thrombelastograph (samples run in triplicates \pm S.D.). The Normal value is the published U.S. calibration value from a pool of blood donors.

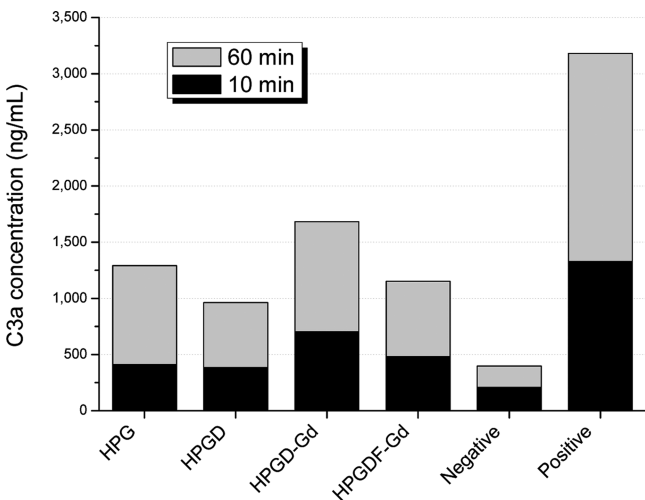


Figure 6. Complement activation in plasma after incubation with different HPGs for 1 h.

time point (Figure 7). In absolute activity uptake into the tumors, the increase from 2.5% of total injected activity in the tumor at 24 h to 6.0% of activity in the tumor at 72 h was 2.4-fold, while the tumors grew in this time only by 1.7-fold, from a volume of 0.22 ± 0.06 mL to 0.38 ± 0.02 mL. Extravasation from leaky tumor vasculature and consequent accumulation in the tumor, also known as the enhanced permeation and retention (EPR) effect,³⁶ might be responsible for this increase. To take advantage of the EPR effect, long-circulating nanocarriers are needed that are not quickly removed from the vasculature by the reticulo-endothelial system (i.e., by

Table 1. Platelet Activation Caused by HPGD and Derivatives (1 mg/mL) in Whole Blood Measured by the CD62 Expression Level in Percentage of Measured Platelets^a

compound	10 min	30 min	60 min
Positive control	$97.0 \pm 0.3\%$	$96.5 \pm 0.1\%$	$95.4 \pm 0.6\%$
Negative control	0.0%	0.0%	0.0%
Platelet measurement	$99.8 \pm 0.1\%$	$99.8 \pm 0.1\%$	$99.8 \pm 0.1\%$
HPG	$5.9 \pm 0.7\%$	$11.0 \pm 1.1\%$	$6.9 \pm 0.9\%$
HPGD	$6.8 \pm 0.5\%$	$12.3 \pm 0.4\%$	$8.3 \pm 0.9\%$
HPGD-Gd	$5.9 \pm 0.2\%$	$10.6 \pm 0.3\%$	$6.6 \pm 0.2\%$
HPGDF-Gd	$6.6 \pm 0.1\%$	$11.0 \pm 0.9\%$	$7.9 \pm 0.9\%$

^aExperiments were done in triplicate \pm S.D.

phagocytosis or excretion). Our HPG derivative described here is clearly such a long-circulating macromolecule.

MR Imaging and Fluorescent Histology Analysis. The HPGD-Gd relaxivity was measured to be $1075 \text{ mM}^{-1} \text{ s}^{-1}$ (Figure 8). The relaxivity of HPGD-Gd was found to be significantly higher than that of the commercially available Galbumin ($r_1 = 82.85 \text{ mM}^{-1} \text{ s}^{-1}$), and conventional commercially available agents (e.g., Bayer Healthcare's Gadovist, $r_1 = 3.58 \text{ mM}^{-1} \text{ s}^{-1}$) (Figure 8). The inset in Figure 8 is a T1-weighted image of 5 vials, each containing a different concentration of HPGD-Gd visually demonstrating the signal contrast achievable in MRI. Assuming similar capacity to facilitate proton relaxation in the free as well as HPGD-Gd, one can estimate a coordination of 200–300 Gd-DOTA molecules per HPG macromolecule. Further, since less HPG may be administered for a similar T1 effect, dosage of HPGDF-Gd administered was not limited by viscosity. The 0.33 mM stock

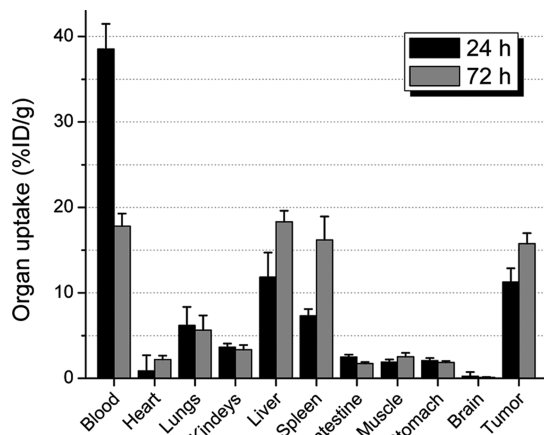


Figure 7. Biodistribution of ^{111}In -HPGD 24 and 72 h after tail vein injection. The percent injected dose per gram of tissue is given \pm SD ($n = 5$).

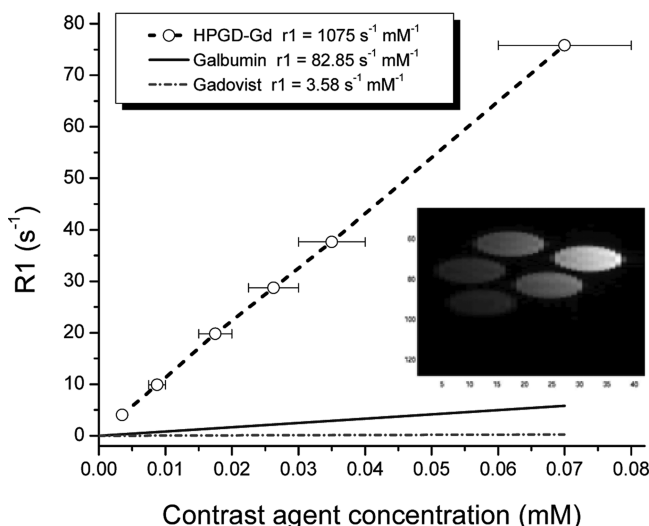


Figure 8. Relaxation rate, R_1 , for HPGD-Gd increases much faster with molar concentration in comparison to galbumin and low-molecular-weight contrast agent Gadovist. Correspondingly, relaxivity, r_1 , is orders of magnitude higher for HPGD-Gd. The graph inset shows a T_1 -weighted MR image of 5 vials with different concentrations of HPGD-Gd, demonstrating image contrast achieved by varying concentrations of the agent.

solution of Galbumin is rather “oily” and cannot easily be more concentrated before injection.

Both R_1 relaxation rate measurements from *in vivo* MRI and subsequent histological analyses of the same tumors show accumulation of HPGDF-Gd to reach a maximum, followed by a slow decrease. Relaxation rate R_1 measurements of tumors receiving HPGDF show a maximum at 3 days post-injection (Figure 9). Compare this to the expected fast peaking and washout using the low-molecular-weight agent Gadovist (black bars) in the same figure. Fluorescence measurements show a maximum between 60 min and 6 days post-injection. The group-averaged fluorescence from histological sections is plotted over a bar graph of relaxation rate $R_1 = 1/T_1$ from MRI data at different time points in Figure 9.

MRI results show heterogeneous signal enhancement following injection of HPGDF-Gd. Figure 10 shows T_1 -weighted RARE MRI images of a tumor (c) prior to and (d) 40

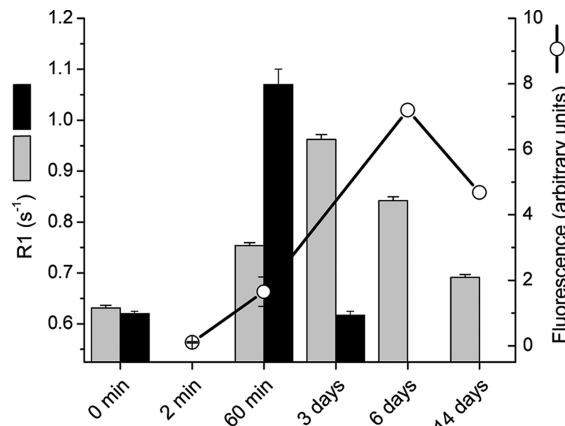


Figure 9. *In vivo* tumor MR R_1 relaxation rate measurements for HPGDF (gray bars) and Gadovist (black bars) are compared to the overlaid corresponding HPGDF fluorescence values (white circles) obtained from histological tumor sections.

min post-injection of HPGDF-Gd, while (a) shows the corresponding histological HPGDF-Gd fluorescence image of the same tumor at 60 min post-injection. The heterogeneous distribution of HPGDF-Gd observed in the MR and histological images is the likely result of variable perfusion, extravasation, and retention known to exist in solid tumors (for a comprehensive review, see Dreher et al.³⁷). These findings warrant further study and will be examined in greater detail in a future publication in combination with other biomarkers of the heterogeneous tumor microenvironment.

CONCLUSIONS

We developed a novel trimodal imaging agent suitable for combined SPECT, MR, and optical imaging. The tested high-molecular-weight HPG was biocompatible, highly soluble, with a long-circulating plasma half-life, and could be labeled with ^{111}In with excellent labeling efficiency and good stability, yielding quantitative biodistribution data. Gd coordination to HPG resulted in an MRI contrast agent with 10-fold enhanced relaxivity relative to that of other macromolecular agents such as the commercially available Galbumin. In *in vivo* experiments, HPG was found to have greater effect on average tumor T_1 than Galbumin. Our biodistribution study and MRI T_1 relaxation measurements demonstrated an increased uptake of HPGs by the tumors over time. Additionally, *ex vivo* fluorescence microscopy of tumors following MRI supported these findings. A heterogeneous distribution of HPGDF-Gd was observed in the MR and histological images, likely due to variable perfusion, extravasation, and retention. This provides additional rationale regarding the importance of distinguishing the physiological parameters of perfusion and permeability measured using MRI and histological methods, which can demonstrate considerable inter- and intratumor heterogeneity. These data could prove valuable for evaluating tumor vascular response to treatment by antiangiogenic or vascular targeting strategies, as well as for interpreting naïve tumor vascular characteristics and consequently effective treatment options. All three imaging modalities combined and overlapped are especially useful in preclinical investigations to yield highly specific and quantitative data regarding tumor vascular function *in vivo*.

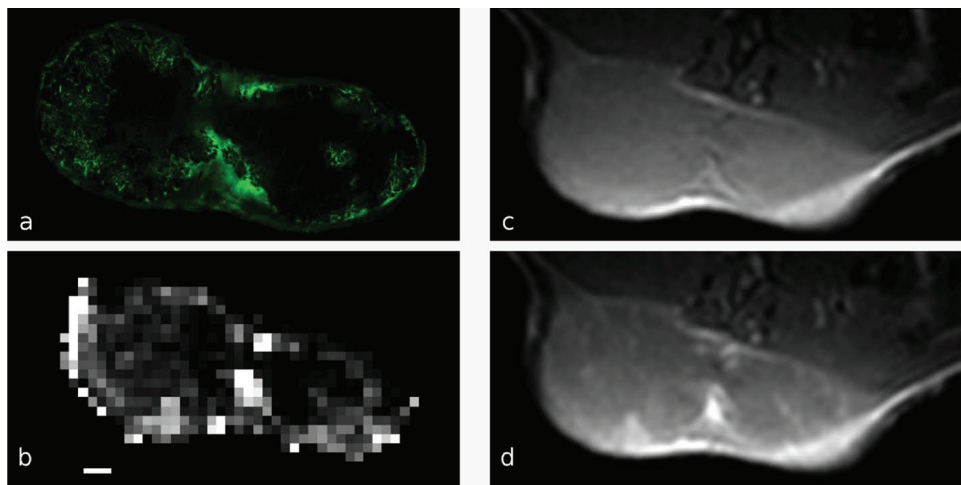


Figure 10. (a) Image of HPGDF-Gd fluorescence of a tumor cryosection. (b) HPGDF-Gd concentration from calibrated change in R_1 relaxation rate (range from 0 to 1 s^{-1}) of the same slice and orientation *in vivo*. Corresponding T1-weighted RARE MR images are shown (c) prior to and (d) 40 min post-injection of 600 mg/kg of HPGDF-Gd. Scale bar indicates 1 mm.

■ ASSOCIATED CONTENT

Supporting Information

Additional ^1H NMR spectra and GPC data of the polymers. This material is available free of charge via the Internet at <http://pubs.acs.org>.

■ AUTHOR INFORMATION

Corresponding Author

*E-mail: urs.hafeli@ubc.ca; Tel. (604) 822-7133; Fax (604) 822-3035.

Notes

The authors declare no competing financial interest.

■ ACKNOWLEDGMENTS

We thank Dr. Dawn Waterhouse for providing us with animals for the ^{111}In biodistribution study. This research was partly funded by a research/operating grant "Alternative radiopharmaceuticals for medical imaging" to UH from both the Canadian Institutes of Health Research (CIHR) and the Natural Sciences and Engineering Research Council of Canada (NSERC). The Canadian Cancer Society and the Canadian Breast Cancer Foundation (JHEB) also supported this study.

■ REFERENCES

- (1) Condeelis, J., and Weissleder, R. (2010) In vivo imaging in cancer. *Cold Spring Harbor Perspectives in Biology* 2, a003848.
- (2) O'Connor, J. P., Jackson, A., Parker, G. J., and Jayson, G. C. (2007) DCE-MRI biomarkers in the clinical evaluation of antiangiogenic and vascular disrupting agents. *Br. J. Cancer* 96, 189–95.
- (3) Tofts, P. S., Brix, G., Buckley, D. L., et al. (1999) Estimating kinetic parameters from dynamic contrast-enhanced T(1)-weighted MRI of a diffusible tracer: standardized quantities and symbols. *J. Magn. Reson. Imaging* 10, 223–32.
- (4) Sunder, A., Hanselmann, R., Mulhaupt, R., and Frey, H. (1999) Controlled synthesis of hyperbranched polyglycerols by ring-opening multibranching polymerization. *Macromolecules* 32, 4240–4246.
- (5) Frey, H., and Haag, R. (2002) Dendritic polyglycerol: a new versatile biocompatible-material. *J. Biotechnol.* 90, 257–67.
- (6) Kainthan, R. K., Muliawan, E. B., Hatzikiriakos, S. G., and Brooks, D. E. (2006) Synthesis, characterization, and viscoelastic properties of high molecular weight hyperbranched polyglycerols. *Macromolecules* 39, 7708–7717.
- (7) Cheng, Y., Zhao, L., Li, Y., and Xu, T. (2011) Design of biocompatible dendrimers for cancer diagnosis and therapy: current status and future perspectives. *Chem. Soc. Rev.* 40, 2673–703.
- (8) Kainthan, R. K., and Brooks, D. E. (2007) In vivo biological evaluation of high molecular weight hyperbranched polyglycerols. *Biomaterials* 28, 4779–87.
- (9) Kainthan, R. K., Hester, S. R., Levin, E., Devine, D. V., and Brooks, D. E. (2007) In vitro biological evaluation of high molecular weight hyperbranched polyglycerols. *Biomaterials* 28, 4581–90.
- (10) Kainthan, R. K., Gnanamani, M., Ganguli, M., et al. (2006) Blood compatibility of novel water soluble hyperbranched polyglycerol-based multivalent cationic polymers and their interaction with DNA. *Biomaterials* 27, 5377–90.
- (11) Kainthan, R. K., Janzen, J., Levin, E., Devine, D. V., and Brooks, D. E. (2006) Biocompatibility testing of branched and linear polyglycidol. *Biomacromolecules* 7, 703–9.
- (12) Hoffman, A. S. (1998) A commentary on the advantages and limitations of synthetic polymer-biomolecule conjugates, in *Biorelated polymers and gels* (Okano, T., Ed.) pp 231–248, Academic Press, Boston.
- (13) Kainthan, R. K., Janzen, J., Kizhakkedathu, J. N., Devine, D. V., and Brooks, D. E. (2008) Hydrophobically derivatized hyperbranched polyglycerol as a human serum albumin substitute. *Biomaterials* 29, 1693–1704.
- (14) Kainthan, R. K., and Brooks, D. E. (2008) Unimolecular micelles based on hydrophobically derivatized hyperbranched polyglycerols: biodistribution studies. *Bioconjugate Chem.* 19, 2231–8.
- (15) Kainthan, R. K., Mugabe, C., Burt, H. M., and Brooks, D. E. (2008) Unimolecular micelles based on hydrophobically derivatized hyperbranched polyglycerols: ligand binding properties. *Biomacromolecules* 9, 886–895.
- (16) Rossi, N. A. A., Constantinescu, I., Brooks, D. E., Scott, M. D., and Kizhakkedathu, J. N. (2010) Enhanced cell surface polymer grafting in concentrated and nonreactive aqueous polymer solutions. *J. Am. Chem. Soc.* 132, 3423–3430.
- (17) Rossi, N. A., Constantinescu, I., Kainthan, R. K., Brooks, D. E., Scott, M. D., and Kizhakkedathu, J. N. (2010) Red blood cell membrane grafting of multi-functional hyperbranched polyglycerols. *Biomaterials* 31, 4167–78.
- (18) Moore, S., and Stein, W. H. (1948) Photometric ninhydrin method for use in the chromatography of amino acids. *J. Biol. Chem.* 176, 367–88.
- (19) Moore, S., and Stein, W. H. (1954) A modified ninhydrin reagent for the photometric determination of amino acids and related compounds. *J. Biol. Chem.* 211, 907–13.

- (20) Lorenzen, A., and Kennedy, S. W. (1993) A fluorescence-based protein assay for use with a microplate reader. *Anal. Biochem.* 214, 346–8.
- (21) Pieters, R., Huismans, D. R., Leyva, A., and Veerman, A. J. P. (1989) Comparison of the rapid automated MTT-assay with a dye exclusion assay for chemosensitivity testing in childhood leukaemia. *Br. J. Cancer* 59, 217–220.
- (22) Alberts, B., Johnson, A., Lewis, J., Raff, M., Roberts, K., and Walter, P. (2008) Renewal by multipotent stem cells: Blood cell formation, *Mol. Biol. Cell*, 5th ed., pp 1450–1462, Garland Science, New York.
- (23) Patrono, C., and Davi, G. (2008) Platelet activation and atherothrombosis - Reply. *N. Engl. J. Med.* 358, 1638–1639.
- (24) Bally, M. B., Mayer, L. D., Hope, M. J., and Nayar, R. (1993) Pharmacodynamics of liposomal drug carriers: Methodological considerations, in *Liposome Technology*, 2nd ed., (Gregoriadis, G., Ed.) pp 27–41, Vol III, CRC Press, Boca Raton.
- (25) Collins, T. J. (2007) ImageJ for microscopy. *Biotechniques* 43, 25–30.
- (26) Haacke, E. M., Brown, R. W., Thompson, M. R., Venkatesan, R. (1999) Magnetic Resonance Imaging: Physical Principles and Sequence Design, Wiley-Liss, New York.
- (27) Dowell, N. G., and Tofts, P. S. (2007) Fast, accurate, and precise mapping of the RF field in vivo using the 180 degrees signal null. *Magn. Reson. Med.* 58, 622–30.
- (28) Abramoff, M. D., Magelhaes, P. J., and Ram, S. J. (2004) Image Processing with ImageJ. *Biophoton. Int.* 7, 36–42.
- (29) Liu, Y., Liu, G., and Hnatowich, D. J. (2010) A brief review of chelators for radiolabeling oligomers. *Materials* 3, 3204–3217.
- (30) Martell, A. E., Motekaitis, R. J., Clarke, E. T., Delgado, R., Sun, Y., and Ma, R. (1996) Stability constants of metal complexes of macrocyclic ligands with pendant donor groups. *Supramol. Chem.* 6, 353–363.
- (31) De Leon-Rodriguez, L. M., and Kovacs, Z. (2008) The synthesis and chelation chemistry of DOTA-peptide conjugates. *Bioconjugate Chem.* 19, 391–402.
- (32) Liu, S. (2004) The role of coordination chemistry in the development of target-specific radiopharmaceuticals. *Chem. Soc. Rev.* 33, 445–61.
- (33) Reichert, D. E., Lewis, J., and Anderson, C. J. (1999) Metal complexes as diagnostic tools. *Coord. Chem. Rev.* 184, 3–66.
- (34) Kobuchi, Y., Ito, T., and Ogiwara, A. (1988) A model for rouleaux pattern formation of red blood cells. *J. Theor. Biol.* 130, 129–145.
- (35) Porter, R. S., Kaplan, J. L., and Homeier, B. P., Eds. (2011) Common Medical Tests: Blood Tests, in *The Merck Manuals Online Medical Library*, Merck & Co., Whitehouse Station, NJ, USA.
- (36) Maeda, H. (2010) Tumor-selective delivery of macromolecular drugs via the EPR effect: background and future prospects. *Bioconjugate Chem.* 21, 797–802.
- (37) Dreher, M. R., Liu, W., Michelich, C. R., Dewhirst, M. W., Yuan, F., and Chilkoti, A. (2006) Tumor vascular permeability, accumulation, and penetration of macromolecular drug carriers. *J. Natl. Cancer Inst.* 98, 335–44.